0 0 0 0 4 2 0 1 3 7 1

Submitted to Journal of Applied Physics

LBL-3167
Preprint c.1

EVAPORATION OF SOLIDS BY LASER PULSES
PART I - IRON

R. A. Olstad and D. R. Olander

August, 1974

Prepared for the U. S. Atomic Energy Commission
under Contract W-7405-ENG-48

For Reference

Not to be taken from this room

LAWRENCE BERKELEY LABORATORY • UNIVERSITY OF CALIFORNIA • BERKELEY

LBL-3167
c.1

DISCLAIMER

This document was prepared as an account of work sponsored by the United States Government. While this document is believed to contain correct information, neither the United States Government nor any agency thereof, nor the Regents of the University of California, nor any of their employees, makes any warranty, express or implied, or assumes any legal responsibility for the accuracy, completeness, or usefulness of any information, apparatus, product, or process disclosed, or represents that its use would not infringe privately owned rights. Reference herein to any specific commercial product, process, or service by its trade name, trademark, manufacturer, or otherwise, does not necessarily constitute or imply its endorsement, recommendation, or favoring by the United States Government or any agency thereof, or the Regents of the University of California. The views and opinions of authors expressed herein do not necessarily state or reflect those of the United States Government or any agency thereof or the Regents of the University of California.

0 0 0 0 4 2 0 1 3 7 2

EVAPORATION OF SOLIDS BY LASER PULSES

PART I - IRON

by R. A. Olstad and D. R. Olander

Inorganic Materials Division of the
Lawrence Berkeley Laboratory and the
Department of Nuclear Engineering of the
University of California
Berkeley, California 94720

ABSTRACT

The laser induced vaporization of iron was studied using a quadrupole mass spectrometer detector. Neutral atoms emitted by thermal processes at the surface were of interest; energetic ions produced by a plasma near the surface were not. Conventional mode laser pulses served as a heat source and the characteristics of the pulses of vaporized atoms reaching the mass spectrometer were determined by time-of-flight analysis of the output signal from this device. The data agreed reasonably well with the predictions of an equilibrium model, in which transient surface vaporization is treated as a sequence of equilibrium stages at each of which Langmuir vaporization with unit condensation coefficient occurs. Agreement between theory and experiment failed at high laser energies because of the outward flow of molten iron from the spot struck by the laser. This cratering phenomenon invalidated the temperature calculation from which the vaporization rate was calculated.

I. INTRODUCTION

The principal effect of a laser striking a solid is heating of the surface. Because heating is sharply delineated in space and time, many practical uses of the laser-solid interaction have been investigated. These applications include welding and cutting of metals, sampling of micron-size surface areas for analysis by optical, mass or nuclear spectroscopy (1) and thin film deposition (2).

Honig (3) has surveyed the mechanisms of the laser-solid interaction. In materials which are opaque to the incident radiation (which is 0.69 μm for a ruby laser), the laser beam acts as a surface heat source and the temperature-time history of the solid during a pulse may be computed by solution of the transient heat conduction equation. The first manifestations of the surface temperature rise are vaporization and melting. Neutral atoms or molecules are emitted into the gas or vacuum around the solid by Langmuir vaporization. If the surface temperature exceeds the melting point of the substrate, rapid vaporization from the melt occurs and the escaping vapor exerts a recoil pressure on the liquid which causes it to flow outward along the surface. This movement of liquid is observable as a crater at the point of impact of the laser. The recoil pressure may even be large enough to eject small globules of the molten material into the gas space (4).

At higher temperatures, emission of thermionic electrons and thermal ions becomes significant. When the ion and electron cloud near the surface becomes dense enough to remove energy from the laser light before the latter reaches the surface, a plasma with

temperatures measured in the tens or hundreds of eV is formed. The energy of the plasma as partially converted to directed kinetic energy of the constituent ions, which are then observed as high velocity, multiply charged particles emanating from the laser-bombarded spot on the solid.

The present study is concerned with the phenomenon occurring in the low surface temperature range described above, where emission consists nearly exclusively of neutral atoms or molecules. Laser power is purposely kept low enough to avoid formation of a plasma and the accompanying energetic ions. Our aim is to determine whether the properties of the emitted particles (composition, energy and rate of vaporization) can be explained by application of equilibrium thermodynamics to the surface temperature transient induced by the laser pulse. The question of vapor composition vis-a-vis the solid composition is important in the use of laser bombardment as a sampling technique. Baldwin (1), for example, found that the deposits collected from laser evaporation of brass contained a higher zinc content than the substrate. However, the zinc concentration of the vaporized samples was that of the <u>liquid</u> in equilibrium with the solid, and not that of the <u>vapor</u> in equilibrium with a condensed phase as might be expected. Other studies have shown that the vaporized material has the same composition as the substrate (5). The noncongruency of the vaporization process appears to be greatest for low incident laser power densities (4), and this is just the region in which the laser pulses produce temperature transients akin to flashing a filament electrically. It is in this region of low surface temperatures where the vaporization process may be reasonably described as a sequence of Langmuir vaporization steps.

In the present paper, the vaporization of pure iron by conventional mode ruby laser pulses is described. In the following paper, we report the results of the evaporation of the binary compound zirconium hydride by Q-switched pulses. Iron vaporization was studied first because this process is considerably simpler than vaporization of a compound, where composition as well as temperature changes in the solid during the laser pulse must be considered. Comparison of theory and experiment for iron vaporization permits the validity of certain aspects of the equilibrium model to be assessed and provides a firm foundation for the study of compound vaporization.

II. EXPERIMENTAL APPARATUS

The apparatus shown in Figure 1 consists of three principal components:

(a) the laser and equipment for measuring laser power and energy.
(b) the vacuum system containing the target and the mass spectrometer.
(c) the signal processing equipment.

The target consists of the machined end of a 4.8 mm diameter rod of high purity polycrystalline iron mounted on a linear feedthrough. The end of the rod is located at the focal plane of the laser, which enters the vacuum system through the window shown in Figure 1. The surface of the target is normal to the axis formed by the mass spectrometer ionizer and the collimating aperture separating the target chamber and the mass spectrometer chamber. The laser strikes the target at an angle of 45° to the surface normal. Since the laser spot is $\sim$ 1 mm in diameter, several shots on fresh surface of the target can be made before repolishing is required.

The target chamber is maintained at 10^{-7} Torr by a 500 lit/sec oil diffusion pump. The mass spectrometer chamber is evacuated by a 200 lit/sec ion pump and a titanium sublimation pump. The pressure in this chamber is $\sim 10^{-9}$ Torr.

As a result of heating by the laser pulse, the target emits atoms or molecules, a small fraction of which pass through the 3.2 mm diameter collimating aperature between the target and mass spectrometer chambers and enter the ionizer cage of a quadrupole mass spectrometer. The flight path between the solid target and the mass spectrometer is 40 cm. The diameter of the collimator between the chambers (3.2 mm) is selected so that the pulse of molecules from the target does not strike the walls of the ionizer, or the ionizer acts as a "once through", density sensitive detector. A small percentage of the neutral particles reaching the mass spectrometer are ionized by electron bombardment, mass analyzed and those of the pre-selected mass number are detected by an electron multiplier. The electron multiplier output current is displayed on an oscilloscope, the x- and y- axes of which represent time and signal amplitude, respectively. This signal trace contains information on the amount and the velocity distribution of a particular species emitted by the target solid due to the incident laser pulse. A brief description of the components of the apparatus is given below. Additional details are available in reference 6.

A. Laser

The laser consists of a 4 in x 9/16 in ruby rod pumped by a helical xenon flashlamp (KORAD KQ-1 system). The optical elements following the output reflector shown in Figure 1 are a beam splitter,

a cell containing an aqueous solution of copper sulphate and a lens with a focal length of 20 cm.

The beam splitter (a glass laboratory slide) reflects a few percent of the incident radiation onto a magnesium oxide block which serves as a diffuse reflector for providing a photodiode (KORAD KD1) with an input signal from which the laser power and total energy in the pulse are determined. The energy signal is observed on a Tektronics Type 585A oscilloscope. The power-time shape of the pulse is determined either by differentiating the energy signal or directly by displaying the power pulse on a Tektronics type 519 oscilloscope. The energy signal output of the photodiode is calibrated using a manufacturer-supplied laser calorimeter (KORAD KJ-2). The power output in the conventional mode consists of a series of triangular spikes each about 0.5 μsec wide and separated by ∿ 1.5 μsec. The average power output (as determined from the derivative of the energy trace) is approximately triangular with the peak occurring at 0.15 msec and ending at 1 msec. Approximately 10 J of energy is contained in the conventional mode pulse.

The copper sulphate cell attenuates the laser radiation and thereby permits variation of the energy incident on the target. The transmissivity of the cell as a function of copper sulphate concentration was calibrated for this purpose.

The focusing lens determines the spot size, and hence the energy per unit area reaching the target. Based upon measurements of the angular divergence of the laser made by the manufacturer, the intensity of the beam as a function of angle θ from the beam

axis is Gaussian of the form $\exp(-\theta^2/\delta^2)$, where $\delta = 2.6$ mrad. This intensity variation in terms of angle θ may be converted to one in terms of radial distance r from the beam axis at the focal plane of the lens. The time and radial dependence of the power density I at the plane is found to be:

$$I(r,t) = \frac{2E}{\pi\sigma^2\tau_2} \exp\left(-\frac{r^2}{\sigma^2}\right) f(t), \quad \text{watts/cm}^2 \qquad (1)$$

where E is the total energy (in joules) in the pulse after attenuation by the copper sulphate cell, the lens and the window. The radial spread is given by $\sigma = f\delta$, where f is the focal length of the lens. For f = 20 cm and $\delta = 2.6$ mrad, $\sigma = 0.052$ cm, so that the incident laser beam is approximately 1 mm in diameter as it strikes the target. f(t) in Eq. (1) represents the triangular temporal shape of the conventional mode pulse averaged over the spikes which constitute this form of lasing:

$$f(t) = \begin{cases} \dfrac{t}{\tau_1} & \text{for} \quad 0 \le t \le \tau_1 \\[2ex] \dfrac{\tau_2 - t}{\tau_2 - \tau_1} & \text{for} \quad \tau_1 \le t \le \tau_2 \\[2ex] 0 & \text{for} \quad t > \tau_2 \end{cases} \qquad (2)$$

Here, $\tau_1 = 0.5$ msec is the time at which the peak energy density occurs and $\tau_2 = 1$ msec is the total duration of the pulse.

B. Mass Spectrometer Calibration

Since our aim is to compare quantitatively the equilibrium theory of vaporization during the laser pulse with measurements, absolute calibration of the mass spectrometer is necessary. When tuned to a convenient isotope of iron (mass 56 was used), this instrument produces an output current pulse S(t) as a consequence of a laser pulse which first impinges on the target at t = 0. We have chosen to compare theory and experiment by converting the output current S(t) to the density of iron atoms in the ionizer of the mass spectrometer n(t) and calculating the latter quantity theoretically from the known characteristics of the laser pulse, the vapor pressure of iron and the geometry of the flight path between the target and the ionizer.

Two steps are involved in obtaining n(t) from the data. First, the instrumental constant relating S and n for a steady state situation must be determined. Second, the time lags inherent in the mass spectrometer and its associated electronics must be accounted for.

In order to determine the instrumental constant,

$$K = S/n \tag{3}$$

the target was replaced by an iron disk heated to a known temperature by electron bombardment and the mass spectrometer output was measured. The disk was masked by a tungsten sheet with a hole of known diameter in the center in order to fix the area of the vapor-

izing iron. According to the theory of Langmuir vaporization, the density of iron atoms in the mass spectrometer ionizer is*:

$$n = \frac{\alpha A P(T)}{4\pi \ell^2 kT} \tag{4}$$

where P(T) is the vapor pressure of iron at the target temperature T (7), A is the area of the iron and ℓ is the distance between the disk and the mass spectrometer. α is the condensation coefficient of iron atoms on an iron surface, which is assumed to be unity (8,9).

By measuring the mass spectrometer output current S at various iron temperatures, calculating the atom density n from Eq. (4) and dividing the two according to Eq. (3), a value $K = 2.8 \times 10^{-16}$ amps/(atom/cm^3) is obtained. This constant can also be calculated from the characteristics of the quadrupole mass spectrometer. It is the product of the ionization cross section for iron atoms by $\sim$ 70 eV electrons, the length of the electron sheet in the ionizer, the electron ionization current, the extraction and transmission efficiencies of the mass spectrometer, the number of secondary electrons produced by impact of an iron ion at the first dynode of the electron multiplier and the gain of the electron multiplier.

*In obtaining Eq. (4), we have neglected the peaking factor, which is the ratio of the actual atomic beam intensity averaged over the electron sheet in the ionizer to the intensity for an unobstructed point cosine source emitting at the same rate. This quantity is less than unity in the present case because the collimating aperture between the disk and the mass spectrometer (Figure 1) prevents the beam of iron atoms from filling the entire ionizer cage. The method of calculating the peaking factor for the present geometry is described in reference 6. Since the peaking factor appears in both the calibration (Eq. (4)) and in the theoretical response (Section IV B), it may be removed from both without affecting the comparison of theory and experiment.

The various components of the theoretical value of K cannot be estimated with sufficient accuracy to warrant comparison with the experimental value of K determined by the calibration procedure just described.

In order to convert transient mass spectrometer signal to the corresponding time-varying atom density in the ionizer, two time lags in the detection process must be considered. The first is the drift time of the ions down the quadrupole structure between the ionizer and the electron multiplier and the second is the RC time constant of the cables, connectors and the oscilloscope. The drift time t_d is easily calculated from knowledge of the length of the quadrupole structure and the accelerating potentials. For an ion of mass 56, t_d = 19 μsec. The RC time constant of the mass spectrometer auxilliary components is measured by examining the shapes of individual pulses from single ion impacts on the first dynode of the electron multiplier. For the circuitry employed, the RC time constant is τ = 30 μsec. Analysis of the electrical network following the electron multiplier for the response due to ions impacting on the first dynode (which impact is delayed by t_d from the time of creation in the ionizer) shows that the transient output is related to the density pulse of iron atoms passing through the ionizer by (6):

$$S(t + t_d) = \frac{K}{\tau} \int_0^t \exp\left(-\frac{t - t'}{\tau}\right) n(t')dt'$$

where K is the instrumental constant determined by the steady state method described earlier. Taking the Laplace transform of the above equation and inverting yields:

$$n(t) = \frac{1}{K}\left\{S(t + t_d) + \tau \frac{d}{dt}\left[S(t + t_d)\right]\right\} \qquad (5)$$

The output signal recorded on an oscilloscope trace is shifted in time by t_d and numerically differentiated. $n(t)$ is then determined from Eq. (5).

III. RESULTS

Pulsing of iron was restricted to conventional mode laser pulses. The mass spectrometer signal due to iron atoms vaporized by Q-switched pulses could not be observed above the background signal at mass 56. The signal produced by the Q-switched pulse is much smaller than that observed in the steady state experiments used to calibrate the mass spectrometer because in the former case, emission occurs in a time period short compared with the transit time of iron atoms from the target to the mass spectrometer. To illustrate this point, compare the signal arising from steady vaporization of the target to that due to a square pulse 40 nsec wide in which the vaporization rate is the same as in the steady state situation. As shall be shown later, the spread of velocities of the iron atoms emitted with a Maxwellian distribution during the pulse leads to a width of the density pulse in the ionizer, $n(t)$, of $\sim$ 400 μsec. Therefore, the average signal from Q-switched pulse vaporization has an amplitude approximately $0.04/400 = 10^{-4}$ times the signal due to the steady state source. Increasing the intensity of the Q-switched mode by using stronger pulses and thereby increasing the surface temperature results in evaporation of energetic iron ions ($\sim$ 30 eV), a phenomenon which is not of interest in the present study. As explained in the introduction,

these pulses are formed in the plasma near the surface, whereas we are interested in direct thermal evaporation of atoms from the surface.

The amplitude of the thermal atom signal arising from conventional mode pulses on iron is $\sim 10^3$ times that obtainable during Q-switched pulses attaining the same peak temperature. In the conventional mode of operation, neutral atoms of thermal energy could be observed without interference from energetic ions. Thermal ions could not be observed because the ionizer of the mass spectrometer is 15 V positive with respect to the target. The ratio of ion to neutral atom emission is given by the Saha-Langmuir equation (3). For iron at 4000°K, this ratio is calculated to be 10^{-4}, so that thermal ions are not expected in our experiments.

Figure 2 shows the output signal of the mass spectrometer tuned to mass 56 following a conventional mode pulse on an iron target. Figure 3 shows the signal after treatment by Eq. (5). Zero time is determined by the triggering of the laser. The ordinate of Figure 3 is proportional to n(t). A summary of the data obtained for pulses of varying energy contents is shown in Table 1. Curves such as the one shown in Figure 3 (which represents the next to the bottom row in Table 1) were analyzed to obtain the salient characteristics of the atom density pulse in the ionizer. A measure of the average transit time of the atoms from the target to the ionizer is given by:

t_{peak} = time at which the maximum atom density is observed

The width of the pulse is represented by:

$t^{\pm}_{\frac{1}{2}}$ = times at which the atom density reaches one half of the maximum value on the rising (-) and falling (+) portions of the pulse in Figure 3.

The maximum amplitude of the pulse is denoted by n_{max} in Table 1. This quantity is dependent upon the accuracy of the instrumental constant K. The average transit time t_{peak} and the half widths of the pulse $t_{peak} - t^-_{\frac{1}{2}}$ and $t^+_{\frac{1}{2}} - t_{peak}$ are independent of the mass spectrometer amplitude calibration. These times depend upon the velocity distribution of the atoms traveling from the target to the mass spectrometer and provide sensitive measures of the temperature of the emitted atoms. The precision of the measured values of t_{peak}, $t^+_{\frac{1}{2}}$ and $t^-_{\frac{1}{2}}$ is approximately $\pm$ 0.04 msec.

IV. THEORY OF EQUILIBRIUM VAPORIZATION DURING A LASER PULSE

A. Surface Temperature

Unfortunately, there is no known method of measuring the temperature of the target surface during the laser pulse. The surface temperature transient $T_s(t)$ must be calculated in order to predict vaporization rates and ultimately the atom density pulse in the ionizer of the mass spectrometer, n(t).

Because the depth of solid involved in heating is much smaller than the spot size of the laser, heat conduction is assumed to occur only in the direction normal to the surface (denoted by x). Because metals are opaque to visible light, the laser radiation is represented by a surface heat source. The adequacy of these two assumptions may be verified analytically by incorporating radial heat flow and a volumetric heat source decaying exponentially in x into simplified solutions of the heat conduction equation (6).

Since the surface recedes because of evaporation, x is defined as the distance from the actual surface rather than from the original surface. In this Lagrangian frame of reference, solid appears to

flow in the negative x direction and a convective term is introduced into the energy equation describing heat transport in the solid. The energy equation for the temperature distribution T(x,t) which includes surface recession and physical property variations is:

$$\frac{\partial T}{\partial t} - \frac{\Phi(T_s)M}{\rho}\left(\frac{\partial T}{\partial x}\right) = \alpha\frac{\partial^2 T}{\partial x^2} + \frac{\alpha}{\kappa}\frac{d\kappa}{dT}\left(\frac{\partial T}{\partial x}\right)^2 \qquad (6)$$

where $\Phi(T_s)$ is the vaporization rate at surface temperature $T_s = T(0,t)$, M is the atomic weight of iron and ρ is its density. The coefficient of $\partial T/\partial x$ in Eq. (6) is the surface recession velocity. α and κ are the thermal diffusivity and thermal conductivity of iron, respectively. Both are known functions of temperature.

Eq. (6) is solved numerically with the following initial and boundary conditions:

$$T(x,0) = T_o \qquad (7)$$

$$T(\infty,t) = T_o \qquad (8)$$

where $T_o = 300°K$ is the initial temperature of the solid. The boundary condition at the vaporizing surface is obtained by a balance of conduction in the solid with heat losses due to the latent heat of vaporization, radiation and heat input from the laser radiation:

$$-\kappa\left(\frac{\partial T}{\partial x}\right)_0 = -\Phi(T_s)\Delta H_{vap} - \varepsilon\sigma_s(T_s^4 - T_o^4) + q(t) \qquad (9)$$

ΔH_{vap} is the heat of vaporization of iron ($\sim$ 97 kcal/gm atom), ε is the emissivity of the surface and σ_s is the Stephan-Boltzmann constant. The vaporization rate is given by:

$$\Phi(T_s) = \frac{P(T_s)}{\sqrt{2\pi MkT_s N_{Av}}}, \quad \text{gm atoms/cm}^2\text{-sec} \tag{10}$$

where N_{Av} is Avogadro's number.

The heat source term q(t) in Eq. (9) is less than the power density in the laser because the radiation is not incident normally upon the surface and because the surface is not perfectly absorbing. For the geometry used in this study, the angle of incidence introduces a factor of cos45° = 0.707. Departure from black body conditions at the surface is accounted for by multiplying Eq. (1) by the emissivity of the surface (which is equal to the absorptivity). Thus,

$$q(t) = 0.707\ \varepsilon I(r,t) = q_p f(t) \tag{11}$$

where

$$q_p = \frac{1.414\ \varepsilon E}{\pi\sigma^2\tau_2} \exp\left(-\frac{r^2}{\sigma^2}\right), \quad \text{watts/cm}^2 \tag{12}$$

is the peak heat flux, which occurs at $t = \tau_1$ during the laser pulse. Because radial transport of heat is neglected in the calculation, the r-dependence of the power density in the laser beam may be treated as constant in solving the energy equation. The radial variation of q_p is considered when the density of iron atoms at the mass spectrometer is computed (next section). The temporal shape of the laser pulse is given by Eq. (2).

Eqs. (6) - (11) were solved numerically for various values of the parameter q_p.

The time variation of the surface temperature for three pulse strengths is shown in Figure 4. The maximum temperature occurs

after the peak of the absorbed power, but the difference in the times of the peak temperature and the peak power diminishes as the latter increases. The curves tend to bunch together as the peak heat flux increases. This effect is due to the rapid increase in the vaporization rate with surface temperature, which renders the latent heat term in Eq. (9) quite comparable to q(t). For example, at the time of the maximum surface temperature for the strongest pulse in Figure 4, the heat input due to laser irradiation is 4×10^5 watts/cm^2. The maximum temperature is 3500°K, for which Eq. (10) gives a vaporization rate of 0.53 gm atoms/cm^2-sec. When this figure is multiplied by the enthalpy of vaporization of iron, the power required to sustain vaporization is 2×10^5 watts/cm^2, which reduces the net surface heat flux by a factor of two when compared to the laser power input alone. Radiation heat losses are totally negligible.

The small bump in the $q_p = 1.7 \times 10^5$ watts/cm^2 curve in Figure 4 is due to the heat released by solidification of iron. Penetration depths of the temperature pulse into the solid are $\sim$ 25 μm for the pulse with $q_p = 3.3 \times 10^5$ watts/cm^2.

The calculations upon which the curves of Figure 4 are based do not consider the individual spikes which comprise the conventional mode laser pulse. This effect was analyzed by calculating the surface temperature transient due to a series of equally spaced triangular power spikes and comparing the vaporization rate due tc this input with that from a surface subjected to a step heat flux input equal to the average heat flux of the sequence of spikes (6).

Since the vapor pressure is an exponentially increasing function of $1/T_s$, the average vaporization rate during one spike is greater than the vaporization rate at the average power input. However, the difference in the calculated vaporization rates is only $\sim$ 10%, so that treatment of the conventional mode pulse in terms of its average power (i.e., using f(t) of Eq. (2)) is deemed adequate. Because of the long atom flight times ($\sim$ 400 μsec) compared to the width of the individual power spikes (0.5 μsec), the mass spectrometer cannot possibly detect the presence of such temporal structure in the vaporization rates arising from the spiked nature of the conventional mode pulse.

B. Atom Density in the Ionizer

An equilibrium model is used to describe the transient vaporization of iron atoms from the surface area struck by the laser pulse. Consider the equilibrium system consisting of solid iron in contact with its equilibrium vapor. The principle of detailed balancing (10) requires that the rate of condensation of vapor atoms in a particular velocity range be equal to the rate of vaporization of the same class of atoms. In accordance with the assumption of unit condensation coefficient for iron atoms on solid iron, the rate of condensation is equal to the rate of impingement of atoms on the surface from the equilibrium gas. The impingement rate is given by multiplying the Maxwell velocity distribution by $v\cos\theta$, where v is the particle velocity and θ is the angle from the surface normal. For the equilibrium system with unit condensation coefficient, the velocity and angular distributions of the vaporized atoms are identical to those of the impinging atoms. When applied to the

non-equilibrium system wherein the solid is exposed to a vacuum and the temperature varies both in time and position in the solid, it is assumed that the vaporization rate is that determined for the equilibrium system at the instantaneous surface temperature. Since our experiment measures emission along the surface normal, $\theta = 0$, the flux of vaporized atoms from an element of surface dA' in the speed range v to v + dv into solid angle $d\Omega$ about $\theta = 0$ is:

$$d\Phi = \frac{P(T_s)}{kT_s}\left(\frac{m}{2\pi kT_s}\right)^{3/2} v^3 \exp\left(-\frac{mv^2}{2kT_s}\right) dv d\Omega dA' \qquad (13)$$

where m is the mass of an iron atom.

We wish to calculate the density of atoms at the mass spectrometer ionizer, which is a distance ℓ from the target, as a function of time during the laser pulse. To do so, it must be recognized that faster atoms arrive at the ionizer before slower ones and that atoms leave the surface at different times during the temperature transient (11). The velocity distribution is converted to a time-of-arrival distribution by setting:

$$v = \frac{\ell}{t - \tau} \qquad (14)$$

where τ is the time of emission of an atom of speed v from the surface and t is the time of its arrival at the downstream position. The difference $t - \tau$ is the transit time of an atom of speed v from the target to the ionizer. Eqs. (13) and (14) are used to obtain the number density n(t) by the following steps:

1) The solid angle $d\Omega$ in Eq. (13) is expressed as $1/\ell^2$, which converts this formula to one giving the flux of atoms per unit area at the ionizer.

2) The flux per unit area is divided by the velocity v to yield the number density.

3) The variable is transformed from v to τ by use of Eq. (14) and by replacing dv by $\ell d\tau/(t - \tau)^2$.

4) The density of atoms of all speeds arising from vaporization from all illuminated areas on the target is obtained by integrating over the target surface (denoted by the polar coordinates r' and ϕ') and over all emission times τ from zero to the arrival time t.

The result is:

$$n(t) = \frac{\ell}{k} \left(\frac{m}{2\pi k}\right)^{3/2} \int_0^{2\pi} d\phi \int_0^{\infty} r'dr' \int_0^{t} \frac{P[T_s(\tau,r',\phi')]}{[T_s(\tau,r',\phi')]^{5/2}(t - \tau)^4} \cdot$$

$$\exp\left\{- \frac{m\ell^2}{2kT_s(\tau,r',\phi')\ (t - \tau)^2}\right\} d\tau \quad (15)$$

The derivation of Eq. (15) implicitly assumes that the atoms move in free flight following emission from the surface and are unaffected by the laser beam through which they must pass en route to the ionizer. Collisions between vaporized atoms in the space close to the surface (where the atom density is high) are neglected. Neither is interaction of the laser beam with the emitted atoms considered in the analysis. Were these phenomena of importance, the equilibrium vaporization model would incorrectly predict the characteristics of atom pulse from the surface and the familiar plasma plume would develop. In order to maintain a sufficiently low vapor density near the surface and avoid atom-atom or atom-laser interactions following vaporization, the surface temperature, and hence the incident laser pulse energy, must be low.

The τ-dependence of the surface temperature in this equation is obtained directly from the solution of the heat conduction equation in the solid presented in the preceeding section. The dependence of T_s or location on the surface stems from the radial spread of the power density of the incident laser beam as expressed by Eqs. (11) and (12). The incident power density is circularly symmetric with the axis of the laser beam, having a functional dependence given by $\exp(-r^2/\sigma^2)$ where r is the radial distance from the beam axis. However, the power density does not depend upon the azimuthal angle about the beam axis, ϕ. Because of the 45° tilt of the target with respect to the laser axis, contours of equal laser energy absorption at the target are elliptical rather than circular. The angular integral in Eq. (15) can be performed directly by converting the spatial coordinates from the (r',ϕ') system on the target surface to the (r,ϕ) coordinates about the laser beam axis. From solid geometry, it can be shown that the coordinate conversion involves merely replacing $r'dr'd\phi'$ by $rdrd\phi/0.707$. Noting that T_s is independent of ϕ, the angular integration yields a factor of 2π. Eq. (15) therefore simplifies to:

$$n(t) = \frac{2\pi}{0.707}\,\frac{\ell}{k}\left(\frac{m}{2\pi k}\right)^{\frac{3}{2}} \int_0^{\infty} rdr \int_0^{t} \frac{P[T_s(\tau,r)]}{[T_s(\tau,r)]^{5/2}(t-\tau)^4} \cdot \exp\left\{-\frac{m\ell^2}{2kT_s(\tau,r)(t-\tau)^2}\right\} d\tau \qquad (16)$$

The calculation proceeds as follows:

1) The incident laser pulse energy E is selected and a value of the surface emissivity ε is assumed.

2) The peak heat flux given by Eq. (12) is computed for various values of r and the heat conduction equation is solved for each of the q_p values as explained in Section IV A. The surface temperature transients are similar to those shown in Figure 4 except that the parameter characterizing each curve is radial coordinate r rather than heat flux q_p and the time variable is τ rather than t.

3) The double integral of Eq. (16) is performed from the calculated function $T_s(\tau,r)$ and the vapor pressure-temperature relation.

We have simplified the numerical work associated with this computation by approximating the r-integral in the following manner. First the radial dependence of the surface temperature is written explicitly in terms of the Gaussian power intensity shape of Eq. (12); that is, we write $T_s(\tau, q_p^\circ e^{-r^2/\sigma^2})$ where:

$$q_p^\circ = \frac{1.414\ \varepsilon E}{\pi\sigma^2\tau_2} \tag{17}$$

is the peak laser heat flux along the beam axis. For a specified value of q_p°, the surface temperature reaches a maximum at time τ_{max} which varies somewhat with q_p (or equivalently, with r). $T_s^{max}(q_p^\circ\ e^{-r^2/\sigma^2})$ denotes the maximum in the temperature-time curve for each radial position r. These are obtained from the maxima of the curves representing solutions of the heat conduction equation, such as those shown in Figure 4. The time integral in Eq. (16) is evaluated at $r = 0$ and the radial variation of the heat flux input is used to define an effective laser spot size. Eq. (16) is approximated by:

$$n(t) = A_{eff} \frac{\ell}{k}\left(\frac{m}{2\pi k}\right)^{\frac{3}{2}} \int_0^t \frac{P[T_s(\tau,q_p^\circ)]}{[T_s(\tau,q_p^\circ)]^{5/2}(t-\tau)^4} \exp\left\{-\frac{m\ell^2}{2kT_s(\tau,q_p^\circ)\ (t-\tau)^2}\right\} d\tau \tag{18}$$

where the effective spot size is defined by:

$$A_{eff} = \frac{2\pi}{0.707} \int_0^\infty \frac{P\left[T_s^{max}(q_p^\circ e^{-r^2/\sigma^2})\right]}{P\left[T_s^{max}(q_p^\circ)\right]} rdr \tag{19}$$

A_{eff} may be computed from the solution to the energy equation as a function of the peak power along the axis. For $q_p^\circ = 1 \times 10^5$ watts/cm^2, $A_{eff} = 0.4 \times 10^{-3}$ cm^2, while for $q_p^\circ = 5 \times 10^5$ watts/cm^2, $A_{eff} = 5.0 \times 10^{-3}$ cm^2. Weighting by use of the vapor pressure in Eq. (19) is, according to Eq. (10), nearly equivalent to weighting by the vaporization rate. Because the vapor pressure is such a strong function of temperature, the portion of the surface closest to the laser beam centerline is heavily favored in the determination of the effective spot size. The spot areas calculated by Eq. (19) are smaller than the value of $\pi(2\sigma)^2 = 8.2 \times 10^{-3}$ cm^2 which characterizes the cross sectional area of the impinging laser beam.

Although Eqs. (18) and (19) do not constitute as accurate a mathematical treatment as does Eq. (16), the computations based upon the simplified method are considerably less tedious. The accuracy of the approximate method is sufficient because it emphasizes the regions of greatest vaporization rates (i.e., at the centerline of the beam in the time integral of Eq. (16) and at the peak temperature for the radial averaging).

The equilibrium model of vaporization by pulsed laser irradiation of a monatomic solid thus consists of calculating n(t) for specific values of ε and E from Eqs. (17) - (19) and the solution of the heat conduction equation. The latter provides the surface temperature transient needed for Eq. (18). Typical time-of-arrival curves n(t) for various q_p^o values are shown in Figure 5. The scale of the ordinate is arbitrary and the shapes of the curves represent the integral in Eq. (18). Note that the peak value of the number density pulse occurs later than either the peak laser power or the peak surface temperature. This delay and the width of the time-of-arrival curve are due to transit from the target to the ionizer of iron atom vaporized with a Maxwell-Boltzmann velocity distribution. The time-of-arrival distributions are broadened because the pulse time τ_2 is comparable to the transit time. n(t) represents a convolution of the function f(t) representing the temporal shape of the laser pulse with the intrinsic spread due to the velocity distribution of the emitted atoms. The similarity between the experimental atom density pulses shown in Figure 3 and the predicted shapes shown in Figure 5 is evident. Quantitative comparison of theory and experiment is based upon the shape, delay and amplitude factors determined from the experimental data and listed in Table 1.

V. COMPARISON OF THEORY AND EXPERIMENT

Figures 6 - 8 compare the atom density pulses in the ionizer determined from the data by use of Eq. (5) (points) with those predicted by application of the equilibrium vaporization model embodied in Eqs. (17) - (19) (curves). Comparison is made on the

basis of the delay time (t_{peak}), the rising and falling half-widths ($t_{peak} - t^{-}_{\frac{1}{2}}$ and $t^{+}_{\frac{1}{2}} - t_{peak}$) and the amplitude ($n_{max}$) of the pulses. The total energy in the laser pulse striking the surface (E) is known for each experiment but calculation of q°_{p} for the theoretical prediction requires specification of the surface emissivity ε as well. Values of this parameter which are approximately the same as literature values provide the most satisfactory fit to the data. Agreement of theory and experiment would be much poorer had the surface been assumed to be perfectly absorbing ($\varepsilon = 1$).

The calculated and experimental values of t_{peak} and ($t_{peak} - t^{-}_{\frac{1}{2}}$) are in good agreement for $\varepsilon \approx 0.5$. The predicted values of n_{max} are larger than the experimental values for emissivities in the expected range 0.4 to 0.5. At low laser energies, the calculated and experimental values of n_{max} are in satisfactory agreement, but for an incident energy of 6.5J the calculated value is approximately an order of magnitude larger than the measured value. There is also a discrepancy between the calculated and measured values of ($t^{+}_{\frac{1}{2}} - t_{peak}$). Agreement is good for the lowest energy pulse (2.4J), but at higher pulse energies, the calculated half width is approximately twice the measured value.

The discrepancies between the calculated and measured values of n_{max} and ($t^{+}_{\frac{1}{2}} - t_{peak}$) can be attributed to the flow of liquid iron. The calcuations were made assuming that the surface remained plane, the only movement being uniform recession due to vaporization. However, when the surface temperature is high and there is a considerable depth of molten iron, the pressure exerted by the vaporizing atoms causes some of the liquid iron to flow to the sides

of the interaction area to form the craters shown in Figure 9. The areas of the central pits measured from these photo micrographs are approximately equal to the A_{eff} values computed from Eq. (19). When the liquid iron flows outward, the iron beneath the surface at the center of the crater is cooler than calculated, so that heat is removed by conduction into the bulk solid more quickly than it would if the radial flow of liquid iron did not occur. This effect causes the actual maximum surface temperature to be less than the calculated values, so the vaporization rate and the amplitude of the atom density pulse are reduced.

Crater formation also causes the surface temperature to decrease at a faster rate than calculated. Since $(t^{+}_{\frac{1}{2}} - t_{peak})$ is largely a measure of the rate at which the surface flux decreases from its maximum value, excessive cooling due to cratering narrows the half-width of the pulse following t_{peak}. $(t^{+}_{\frac{1}{2}} - t_{peak})$ is determined both by the duration over which iron atoms are emitted and by the spread in velocities of the emitted atoms. If the flux of iron atoms at the surface decreases more rapidly than calculated (i.e., the emission pulse becomes more like a delta function), the half-width $(t^{+}_{\frac{1}{2}} - t_{peak})$ will be due solely to the spread of velocities of the emitted atoms. The observed value of $(t^{+}_{\frac{1}{2}} - t_{peak})$ of $\sim$ 0.2 msec is approximately the half width due to the spread of velocities from an effusive Maxwellian source, which supports the above explanation of the effect of cratering on the pulse shape.

The measured and calculated values of the rising half width $(t_{peak} - t^{-}_{\frac{1}{2}})$ are in tolerable agreement, which indicates that the

rate of increase of the surface temperature (and therefore flux of iron atoms from the surface) takes place before appreciable outward flow of molten iron has occurred.

VI. CONCLUSIONS

Despite the discrepancies discussed above, the data conform to the general features of the equilibrium model of solid vaporization by laser pulses; the amplitude of the atom density pulse increases rapidly with laser pulse energy as long as cratering is not severe; the delay time of the maximum of the atom pulse decreases as the energy of the laser pulse is increased; the rising half-width of the atom pulse is relatively insensitive to laser energy as predicted by the theory.

The failure of the theory at the highest energy laser pulse used in the present study (particularly the 6.5J pulse in Figure 8) can be rationalized by the phenomenon of cratering. Formation of a plasma plume does not appear to be significant for iron over the range of laser pulses employed here, although this phenomenon is observed with high energy Q-switched pulses.

The present investigation represents an attempt to predict the nature of thermal atom vaporization from a simple solid in terms of transient Langmuir vaporization driven by a surface temperature transient calculated from the laser input power and the macroscopic theory of heat conduction. The theory contains no adjustable parameters, and our object here was to assess the accuracy of the theoretical predictions for a substance of known vapor pressure. It would be of interest to apply this technique to a solid whose vapor pressure is unknown. The characteristics of

the atom density pulse detected by the mass spectrometer could be used, in conjunction with the theory based upon equilibrium vaporization, as a means of measuring the vapor pressure-temperature relation for the solid. Uranium dioxide is an example of a substance whose vapor pressure in the liquid range is impossible to measure by classical methods. However, before the goal of utilizing pulsed laser vaporization as a vapor pressure measurement method can be realized, several obstacles must be overcome:

1) A quantitative model of the effect of radial flow of molten solid from the center of the laser spot on the time and radius dependence of the surface temperature must be formulated and incorporated into the heat conduction equation. Alternatively, a more powerful laser than the one used in the present experiments must be employed. If E were $\sim$ 100 J, for example, the same energy density obtainable with the present 10 J laser could be obtained over a spot $\sqrt{10}$ greater than the present requirement. Inasmuch as cratering is an edge phenomenon, the center of the spot would be less subject to the undesirable cooling due to liquid flow than was the case in the present experiment.

2) The equilibrium theory depends upon knowledge of the magnitude of the condensation coefficient α and its temperature dependence. For metals this quantity is very close to unity, but for nonmetallic solids, the condensation coefficient is often quite a bit smaller than unity. It may be possible to determine the condensation coefficient from steady state Langmuir vaporization studies at temperatures where the vapor pressure is known and extrapolate the $\alpha(T)$ data so obtained to the high temperature region where $P(T)$ is unknown. Otherwise, only the product $\alpha(T)P(T)$ can be determined experimentally.

3) In the temperature range where the vapor pressure is unknown, the latter must be small enough to avoid formation of an ionized plasma in front of the solid. Were this to occur, no theory is available to deduce P(T) from the characteristics of the pulse of vaporized energetic ions.

This work was done under the auspices of the U. S. Atomic Energy Commission.

TABLE 1

Results of Mass Spectrometer Analysis of Conventional Mode Pulses on an Iron Target

E (joules)	t_{peak} (msec)	$t_{peak} - t^{-}_{1/2}$ (msec)	$t^{+}_{1/2} - t_{peak}$ (msec)	$n_{max} \times 10^{-9}$ (atoms/cm^3)
2.4	1.00	0.25	0.28	0.17
3.5	0.75	0.24	0.19	9.0
3.6	0.70	0.22	0.25	5.5
3.6	0.69	0.18	0.18	10.2
3.7	0.75	0.22	0.15	3.6
3.7	0.79	0.27	0.15	6.3
3.8	0.84	0.29	0.09	6.3
3.8	0.72	0.23	0.20	5.3
3.8	0.75	0.25	0.22	5.2
6.5	0.55	0.20	0.19	40.6

0 0 0 0 4 2 0 1 3 8 5

REFERENCES

1. J. M. Baldwin, Appl. Spectroscopy 24, 429 (1970).
2. H. Schwarz in "Laser Interactions" (Ed. by H. Schwarz and H. Hora), p. 71, Plenum Press (1971).
3. R. E. Honig, ibid., p. 85.
4. J. M. Baldwin, J. Appl. Phys. 44, 3362 (1973).
5. J. K. Kliwer, J. Appl. Phys. 44, 490 (1973).
6. R. A. Olstad, USAEC Report LBL-1177 (1972).
7. A. N. Nesmeianov, "Vapor Pressure of the Chemical Elements", (R. Gary, Ed.), Elsevier (1963).
8. G. A. Somorjai, Adv. in High Temp. Chem. (L. Eyring, Ed.), 2, 203 (1969).
9. G. H. Rosenblatt, et al., in "The Structure and Chemistry of Solid Surfaces" (G. A. Somorjai, Ed.), p. 38-3, Wiley (1969).
10. F. Reif, "Fundamentals of Statistical and Thermal Physics", p. 384, McGraw-Hill (1965).
11. H. Saltsburg, J. Chem. Phys. 42, 1303 (1965).

FIGURE CAPTIONS

Figure 1 Schematic of experimental apparatus: The three regions separated by the dashed lines are (a) laser equipment for measuring laser power and energy; (b) vacuum system containing the target and mass spectrometer; (c) the mass spectrometer signal processing equipment.

Figure 2 Typical mass spectrometer output, S(t), following a conventional mode pulse on an iron target. The horizontal scale is 0.5 msec/division. (The circle at the origin is due to a malfunction of the oscilloscope).

Figure 3 Measured atom density in ionizer, n(t), obtained by treating data such as those in Figure 2 according to Eq. (5).

Figure 4 Calculated surface temperature transients for pulses of various strengths.

Figure 5 Calculated atom density pulse at the ionizer for laser pulses of various strengths.

Figure 6 Comparison between the experimental and calculated values of the pulse delay time.

Figure 7 Comparison between the experimental and calculated values of the pulse half-widths.

Figure 8 Comparison between the experimental and calculated pulse amplitudes.

Figure 9 Craters produced by conventional mode laser pulse on iron. Top: E = 2.2J; Bottom: E = 3.5J.

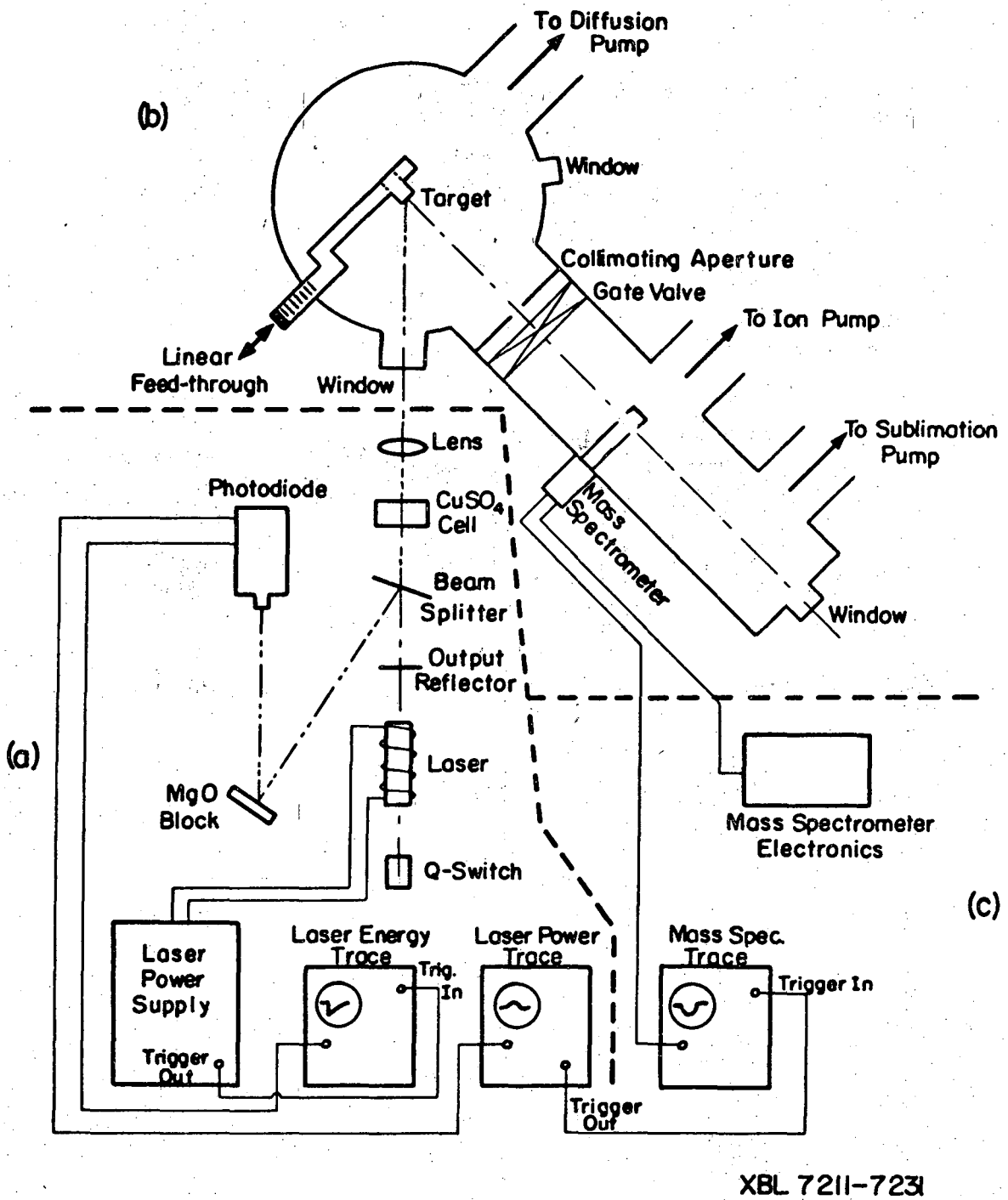
To Diffusion Pump
(b)
Window
Target
Collimating Aperture
Gate Valve
To Ion Pump
Linear Feed-through
Window
To Sublimation Pump
Lens
Photodiode
CuSO4 Cell
Mass Spectrometer
Beam Splitter
Window
Output Reflector
(a)
Laser
MgO Block
Mass Spectrometer Electronics
Q-Switch
(c)
Laser Power Supply
Trigger Out
Laser Energy Trace
Trig. In
Laser Power Trace
Trigger Out
Mass Spec. Trace
Trigger In
XBL 7211-7231

Fig. 1

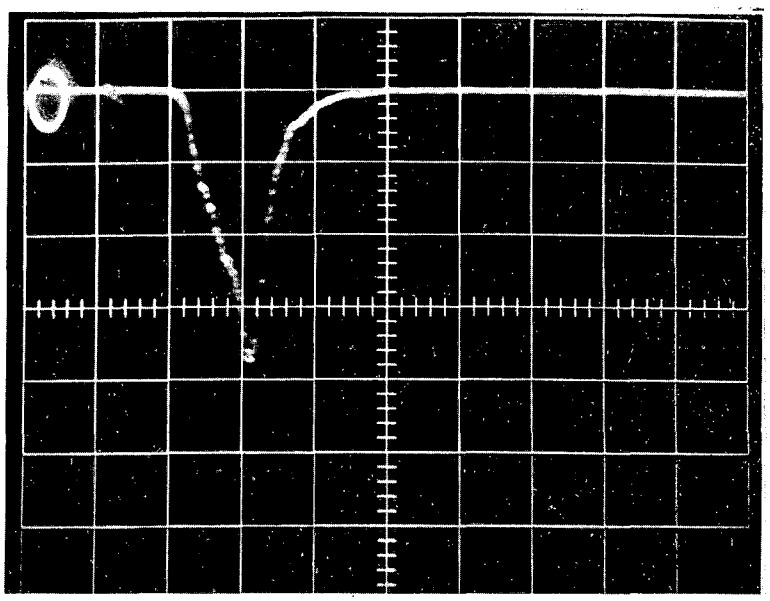

XBB 7210-5370

Fig. 2

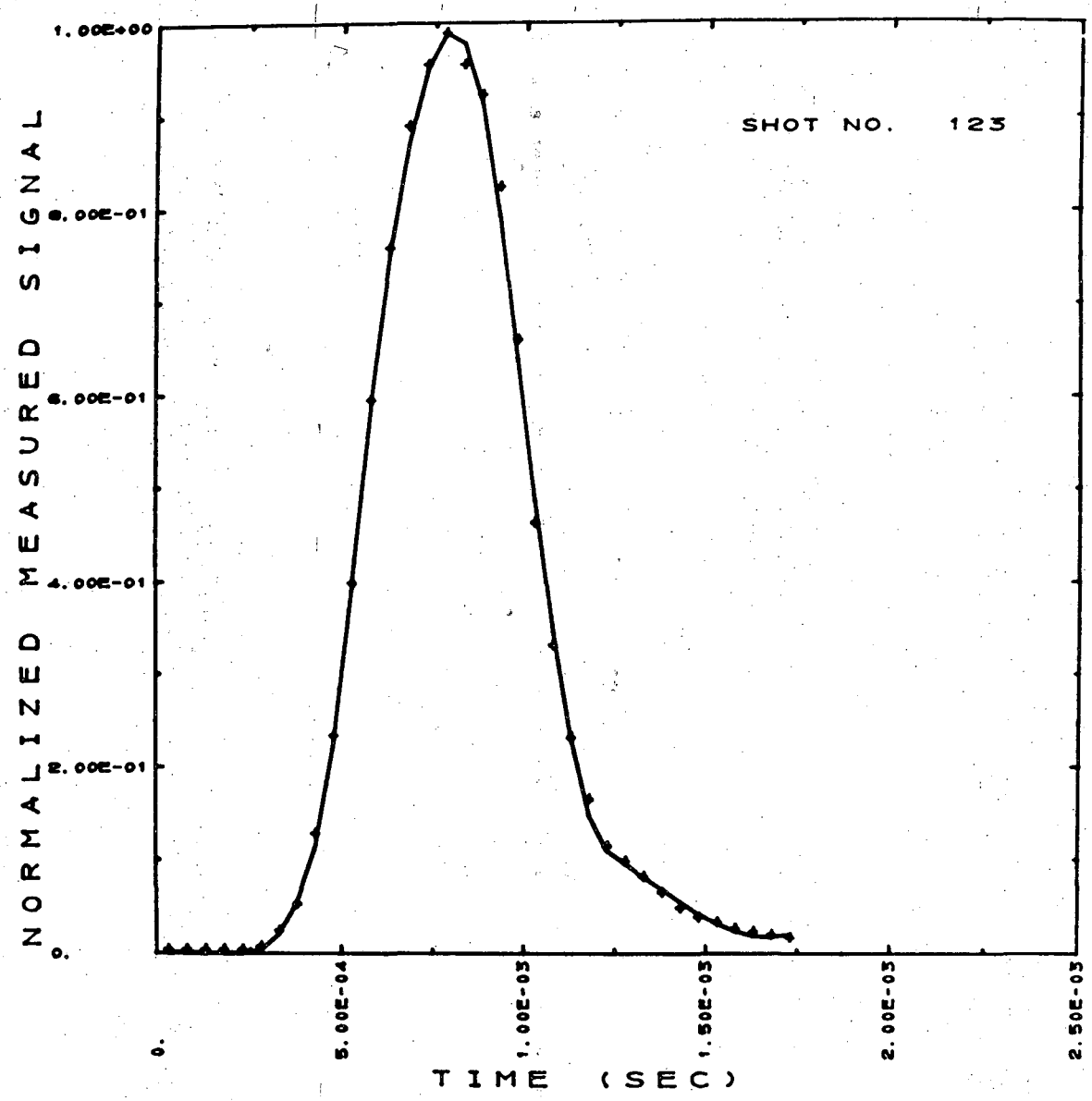

XBL 7210-5784

Fig. 3

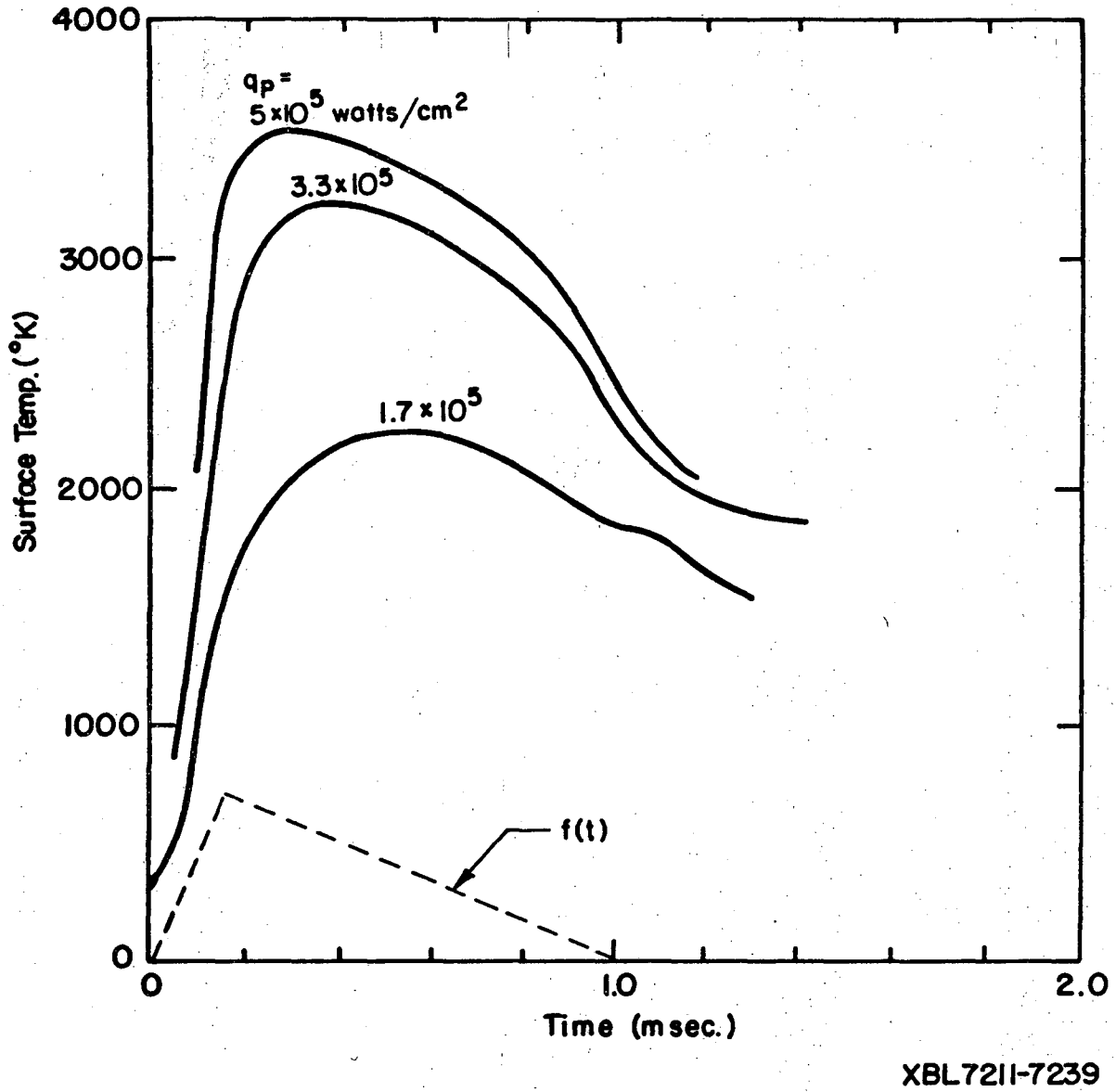
4000
3000
2000
1000
0
Surface Temp. (°K)
q_p =
5×10^5 watts/cm^2
3.3×10^5
1.7×10^5
f(t)
0
1.0
2.0
Time (msec.)
XBL7211-7239

Fig. 4

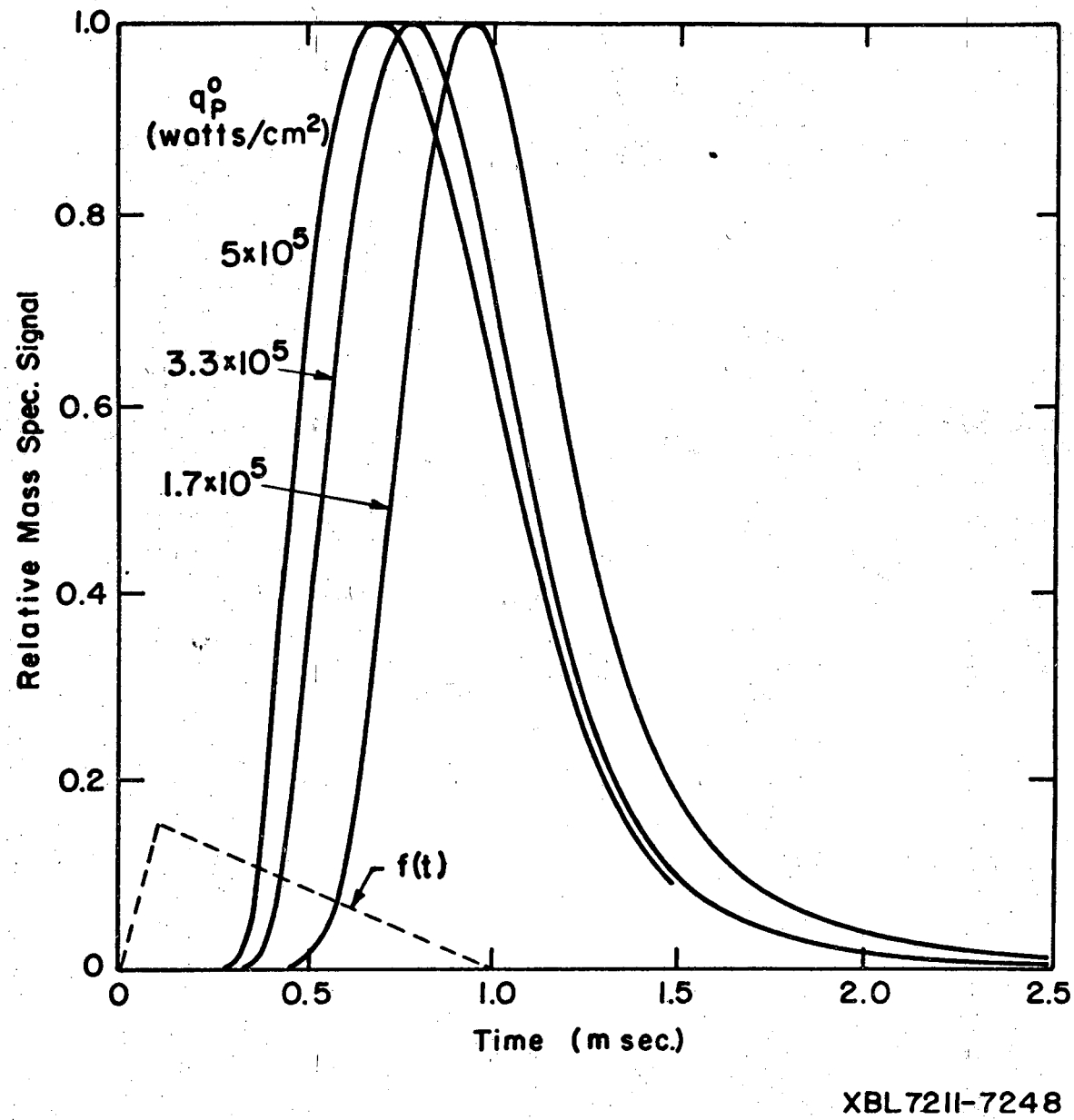
1.0
0.8
0.6
0.4
0.2
0
Relative Mass Spec. Signal
q_p^o
(watts/cm²)
5×10⁵
3.3×10⁵
1.7×10⁵
f(t)
0
0.5
1.0
1.5
2.0
2.5
Time (m sec.)
XBL7211-7248

Fig. 5

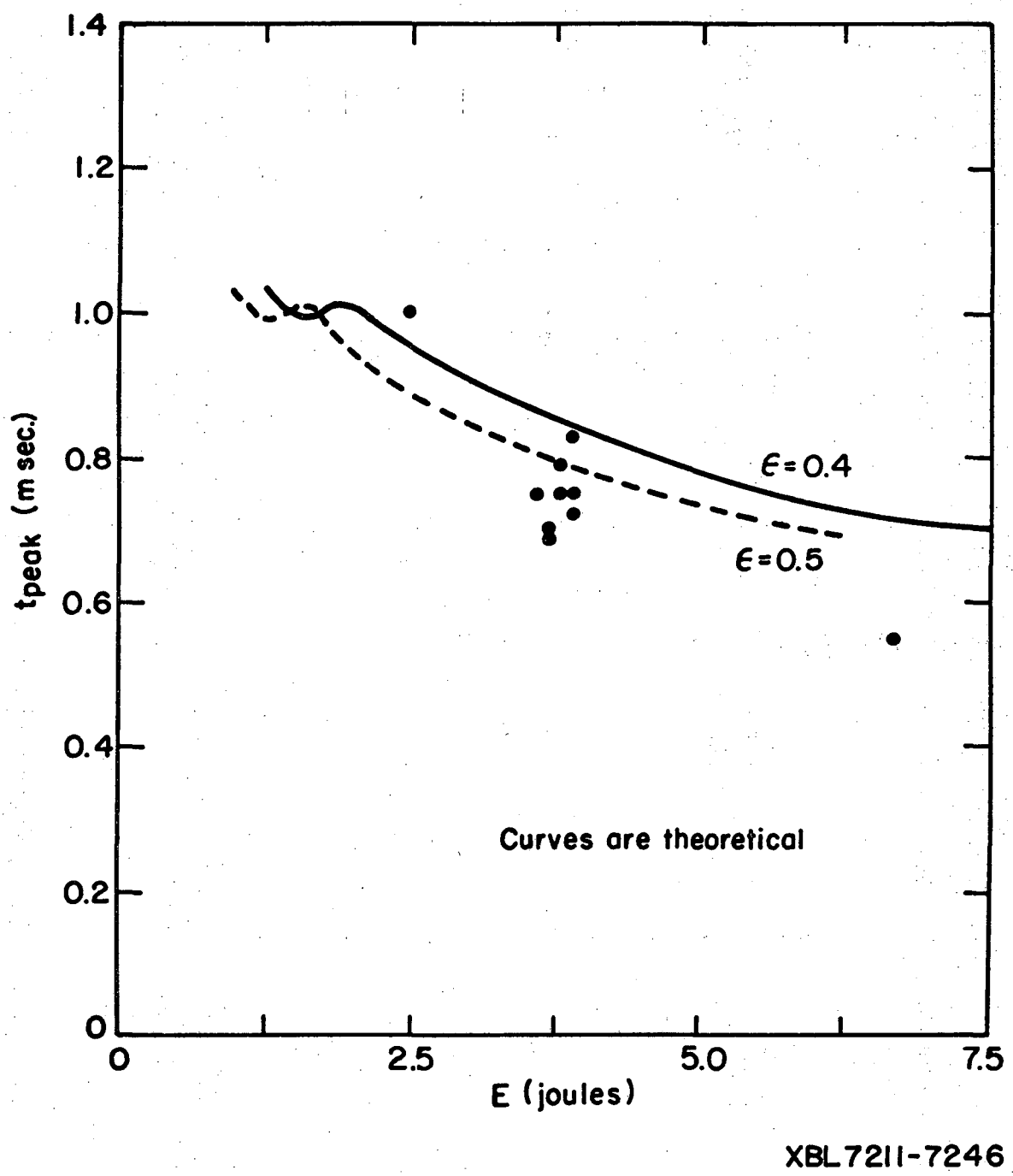
1.4
1.2
1.0
0.8
0.6
0.4
0.2
0
t_{peak} (m sec.)
0
2.5
5.0
7.5
E (joules)
ϵ=0.4
ϵ=0.5
Curves are theoretical
XBL7211-7246

Fig. 6

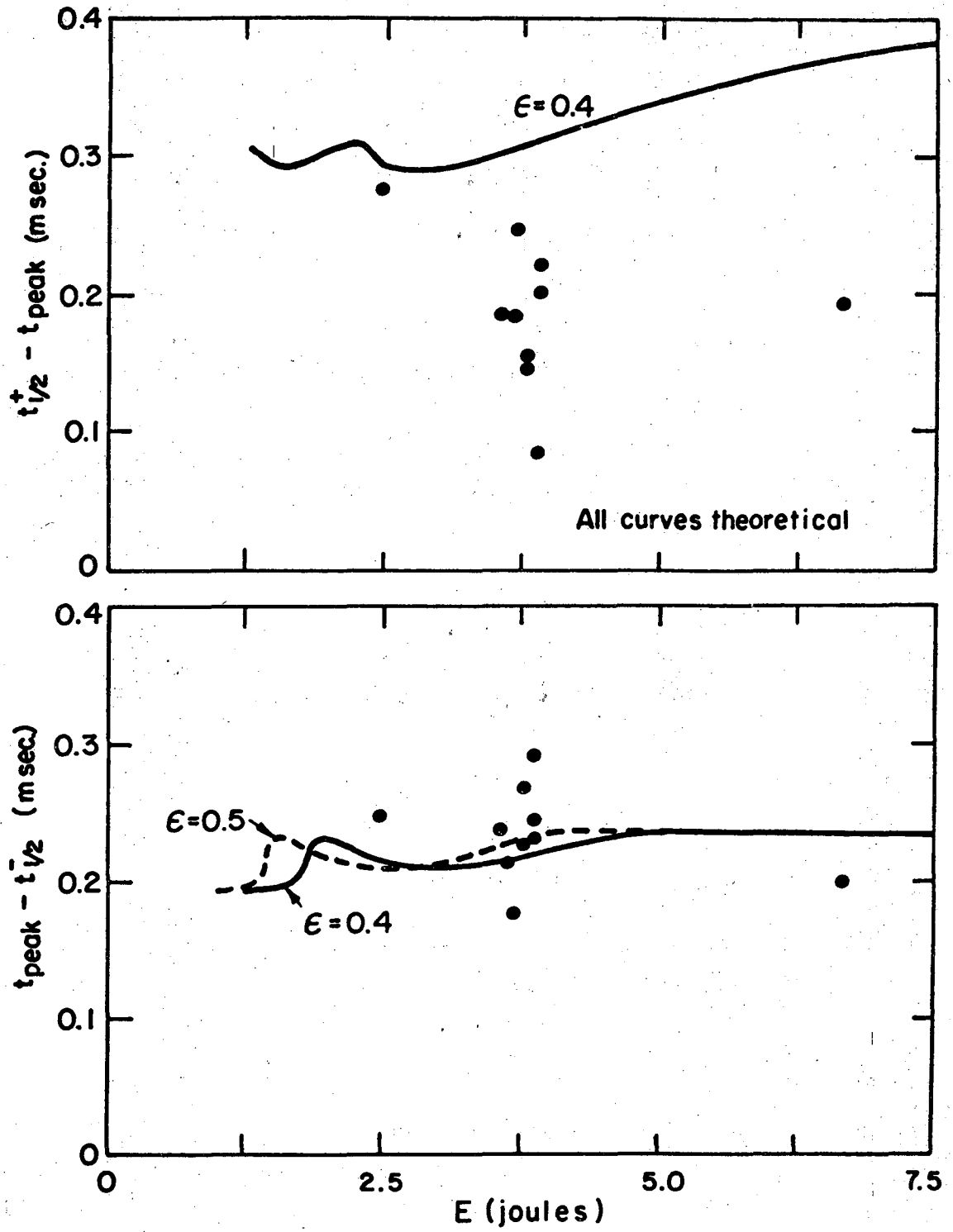

XBL 7211-7244

Fig. 7

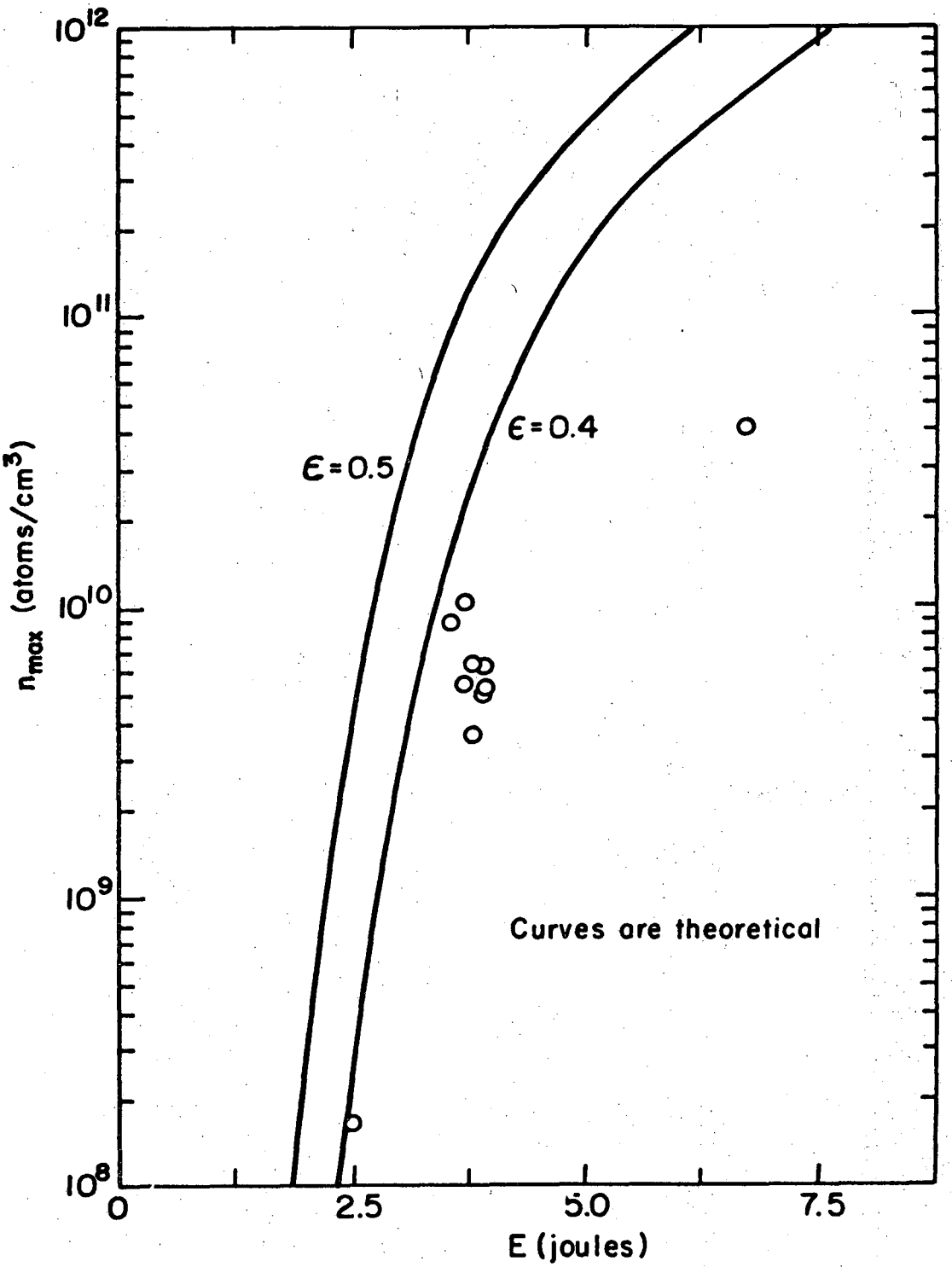

XBL 7211-7250

Fig. 8

0 0 0 0 4 2 0 1 3 9 0

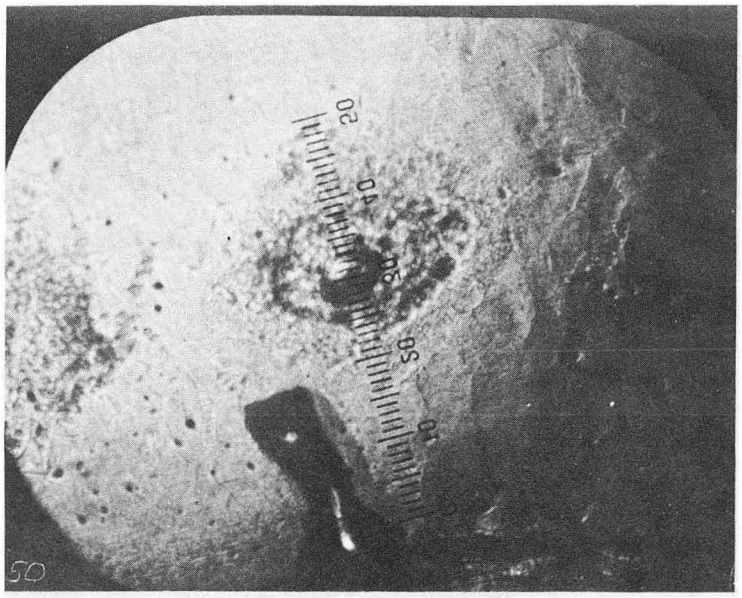

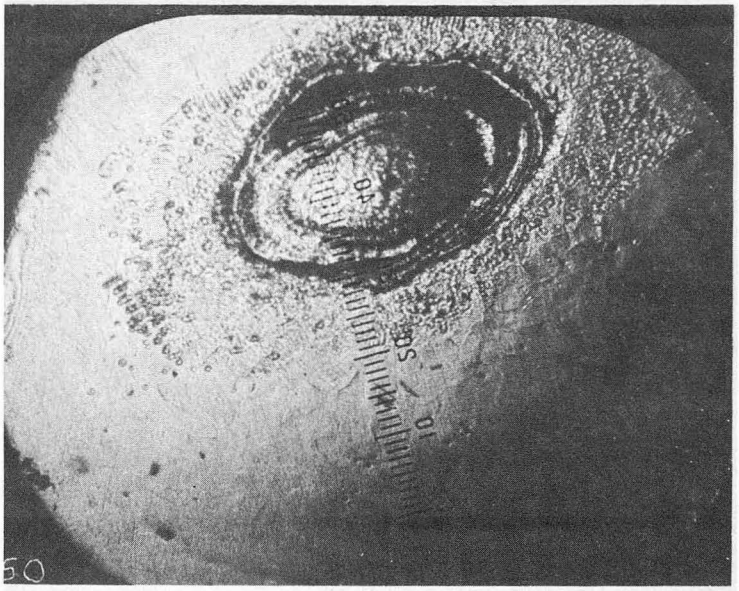

XBB 7210-5373

Fig. 9

LEGAL NOTICE

This report was prepared as an account of work sponsored by the United States Government. Neither the United States nor the United States Atomic Energy Commission, nor any of their employees, nor any of their contractors, subcontractors, or their employees, makes any warranty, express or implied, or assumes any legal liability or responsibility for the accuracy, completeness or usefulness of any information, apparatus, product or process disclosed, or represents that its use would not infringe privately owned rights.

TECHNICAL INFORMATION DIVISION
LAWRENCE BERKELEY LABORATORY
UNIVERSITY OF CALIFORNIA
BERKELEY, CALIFORNIA 94720